

# Assessment of 4-aminoantipyrine degradation and mineralization by photoelectro-Fenton with a BDD anode: Optimization, treatment in municipal secondary effluent, and toxicity

Lucas de Melo da Silva,<sup>[a]</sup> Fábio Gozzi,<sup>[a]</sup> Rodrigo Pereira Cavalcante,<sup>[a]</sup> Silvio César de Oliveira,<sup>[a]</sup> Enric Brillas,<sup>[b]</sup> Ignasi Sirés,<sup>\*[b]</sup> and Amílcar Machulek Junior<sup>\*[a]</sup>

**Abstract:** 4-Aminoantipyrine (4-AA), a persistent metabolite of dipyrone found in natural water, has been treated in 100 mL of aqueous 0.050 M Na<sub>2</sub>SO<sub>4</sub> solutions at pH 3.0 by photoelectro-Fenton (PEF) with a 4 W UVA light. The assays were performed in a cell equipped with a BDD anode and an air-diffusion cathode for H<sub>2</sub>O<sub>2</sub> generation. The formation of an unstable Fe(III)-4-AA complex with 1:2 molar ratio was evidenced. A 2<sup>d</sup> central composite design was used to assess the effect of four independent variables on PEF performance. The optimized conditions for 62.5 mg L<sup>-1</sup> 4-AA were: current density of 77.5 mA cm<sup>-2</sup> and 47.75 mg L<sup>-1</sup> Fe<sup>2+</sup>, yielding 99% 4-AA degradation at 7 min, and 45% 4-AA mineralization with 3.2% mineralization current efficiency at 130 min. Slightly slower degradation and similar mineralization were obtained under these conditions when 4-AA was spiked into a municipal secondary effluent, showing a low influence of natural organic matter on PEF. The initially high acute toxicity determined using *Artemia salina* was largely diminished upon PEF treatment.

most common primary metabolite is 4-aminoantipyrine (4-AA), which has been detected up to 27 µg L<sup>-1</sup> in sewage treatment systems.<sup>[2,3]</sup> 4-AA (C<sub>11</sub>H<sub>13</sub>N<sub>3</sub>O, *M* = 203.24 g mol<sup>-1</sup>) is a *N*-heteroaromatic molecule with a 4-aminopyrazolone group bonded to a benzene ring. The beneficial biological activity of 4-AA has been demonstrated. For example, it allows treating viral diseases<sup>[6]</sup> as well as the formation of stable iron complexes, e.g., with hemoglobin to lower blood flow,<sup>[7]</sup> although it can produce agranulocytosis, i.e., suppression of the immune system.<sup>[8]</sup> The removal of 4-AA has been studied by different technologies including ozonation<sup>[9]</sup> and several advanced oxidation processes (AOPs) such as UV/H<sub>2</sub>O<sub>2</sub>,<sup>[1]</sup> photoelectrocatalysis with TiO<sub>2</sub>/ITO anode,<sup>[10]</sup> and electrochemical oxidation (EO) with boron-doped diamond (BDD).<sup>[11]</sup> AOPs seem highly promising for treating drugs because they produce strong oxidizing species like hydroxyl radical (\*OH) and other reactive oxygen species (ROS), leading to mineralization of most organic pollutants in water.<sup>[4,12-14]</sup>

## 1 Introduction

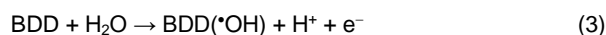
The inefficient destruction of drugs and their metabolites in municipal wastewater treatments plants (WWTPs) using physicochemical and biological processes is a major cause of accumulation and persistence of such organic pollutants in the aquatic environment.<sup>[1-3]</sup> Great social alarm has been created by the presence of these compounds, even trace amounts, in water streams due to their potentially harmful effects on the entire ecosystem, particularly on humans and animals.<sup>[4,5]</sup> Hence, powerful oxidation processes must be developed to ensure their complete removal from wastewater.

Dipyrone (metamizole) is a ubiquitous antipyrine compound, widely prescribed as anti-inflammatory and analgesic drug. Its

Photoelectro-Fenton (PEF) is one of the most powerful electrochemical AOPs (EAOPs). It is a sequential or hybrid process in which the oxidation power of \*OH generated on site is synergistically combined with the photolytic ability of UVA photons.<sup>[15-18]</sup> In this method, H<sub>2</sub>O<sub>2</sub> is continuously produced at a suitable cathode from two-electron reduction of O<sub>2</sub> gas via reaction (1). Then, \*OH is formed in the bulk upon catalyzed H<sub>2</sub>O<sub>2</sub> decomposition with added Fe<sup>2+</sup> via Fenton's reaction (2):<sup>[19-23]</sup>



Carbonaceous cathodes are known to possess the highest electrocatalytic ability for the promotion of reaction (1), thus yielding an excellent current efficiency. Among these materials, carbon nanotubes,<sup>[24,25]</sup> carbon sponge,<sup>[26]</sup> and carbon or graphite felt,<sup>[27-30]</sup> as well as carbon-PTFE fitted into air-diffusion devices<sup>[31-36]</sup>, are the most widely employed. On the other hand, heterogeneous \*OH can be formed on the anode surface from water discharge at high current. The most powerful anodes are the boron-doped diamond (BDD) thin films due to their large O<sub>2</sub>-evolution overpotential and small interaction with heterogeneous \*OH, yielding highly reactive BDD(\*OH) as follows:<sup>[17,21,34]</sup>

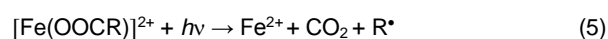


[a] Mr. L.M da Silva, Dr. F. Gozzi, Dr. R.P. Cavalcante, Prof. S.C. de Oliveira, Prof. A. Machulek Jr.  
Institute of Chemistry,  
Federal University of Mato Grosso do Sul  
Av. Senador Filinto Muller, 1555, CP 549, Campo Grande, MS  
79074-460, Brazil  
E-mail: machulekjr@gmail.com

[b] Prof. E. Brillas, Prof. I Sirés  
Departament de Química Física  
Facultat de Química, Universitat de Barcelona  
Martí i Franquès 1-11, 08028 Barcelona, Spain  
E-mail: i.sires@ub.edu

Supporting information for this article is given via a link at the end of the document.

Apart from the oxidation with homogeneous and heterogeneous  $\cdot\text{OH}$  formed from reaction (2) and (3), respectively, in an undivided cell, the UVA radiation in PEF allows the additional destruction of organic matter by different ways: (i) generation of larger  $\cdot\text{OH}$  amounts via reaction (4), with  $\text{Fe}^{2+}$  regeneration, upon  $[\text{Fe}(\text{OH})]^{2+}$  photoreduction, (ii) direct photolysis of photosensitive pollutants, and (iii) photodecomposition of Fe(III) complexes with some *N*-derivatives and carboxylic acids according to the general reaction (5).<sup>[16,19,21,31-36]</sup>



When the solution is not exposed to light, the method is called electro-Fenton (EF), with  $\cdot\text{OH}$  and BDD( $\cdot\text{OH}$ ) acting as the main oxidants. In the absence of  $\text{Fe}^{2+}$  catalyst, the treatment is known as electro-oxidation (EO) with electrogenerated  $\text{H}_2\text{O}_2$  (i.e.,  $\text{EO-H}_2\text{O}_2$ ), being less powerful since homogenous  $\cdot\text{OH}$  is not produced.<sup>[19,21,37,38]</sup> Recent advances on the application of EF and PEF processes have demonstrated the superiority of BDD over other anodes (Pt and DSA<sup>®</sup>) for the removal of drugs.<sup>[23,39-42]</sup>

This work aims to assess the oxidation power of PEF with a BDD anode and air-diffusion cathode to degrade and mineralize 4-AA. The drug was spiked into pure water or a municipal secondary effluent, always in the presence of 0.050 M  $\text{Na}_2\text{SO}_4$  as supporting electrolyte to ensure high conductivity. First, the possible complexation of the drug with  $\text{Fe}^{2+}$  and  $\text{Fe}^{3+}$  and its influence on PEF performance was examined. Then, a  $2^4$  central composite design (CCD) was applied to optimize the current density, initial  $\text{Fe}^{2+}$  and 4-AA concentrations, and time using the pure water matrix. Three responses, namely the percentages of 4-AA degradation, 4-AA mineralization, and mineralization current efficiency (MCE) were considered. The best conditions were applied for treating 4-AA spiked into the real water matrix. The time course of the acute toxicity was assessed in the latter matrix by monitoring the mortality of *Artemia salina* larvae.

## 2 Results and Discussion

### 2.1 Complexation of 4-AA with Fe(III)

Several publications have described the formation of complexes of Fe(III) with several drugs, including 4-AA.<sup>[43-46]</sup> To clarify the potential influence of this complex on PEF treatment, a preliminary spectrophotometric study was carried out within the visible range using a solution with 0.246 mM 4-AA and a much larger content (0.984 mM) of  $\text{Fe}^{3+}$ , at pH 3.0 under dark conditions. Figure 1a highlights the appearance of a wide band between 450 and 650 nm, with  $\lambda_{\text{max}} = 525$  nm, after only 3 min from mixture preparation, which is due to the formation of a Fe(III)-4-AA

complex. However, this complex showed a large instability, as confirmed from the drastic absorbance decay at 10 min.

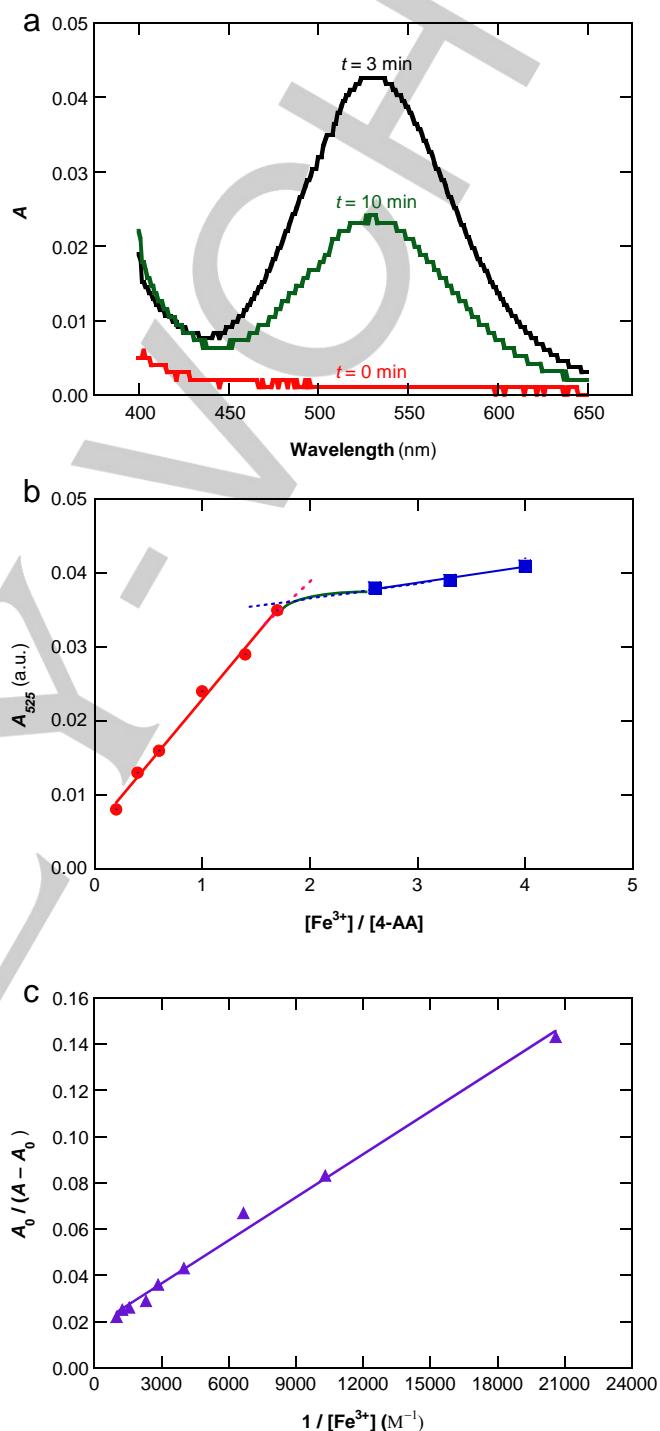


**Figure 1.** (a) Visible spectra of a solution with 0.246 mM 4-aminoantipyrine (4-AA) and 0.984 mM  $\text{Fe}^{3+}$  in the dark, at different times. (b) Absorbance at  $\lambda = 525$  nm, determined 3 min after the preparation of fresh solutions containing 0.246 mM 4-AA and different amounts of  $\text{Fe}^{3+}$ , vs.  $[\text{Fe}^{3+}]/[4\text{-AA}]$  molar ratio. (c) Variation of  $A_0/(A - A_0)$  with the reciprocal of  $[\text{Fe}^{3+}]$  for the assays shown in (b).

When the same experiment was performed under UVA irradiation with a 4-W lamp, the absorption band practically disappeared, thus revealing the photoactivity of the complex (not shown). Conversely, it was confirmed that  $\text{Fe}^{2+}$  is unable to form a complex

with the drug, because the visible spectrum of a 4-AA did not change upon  $\text{Fe}^{2+}$  addition.

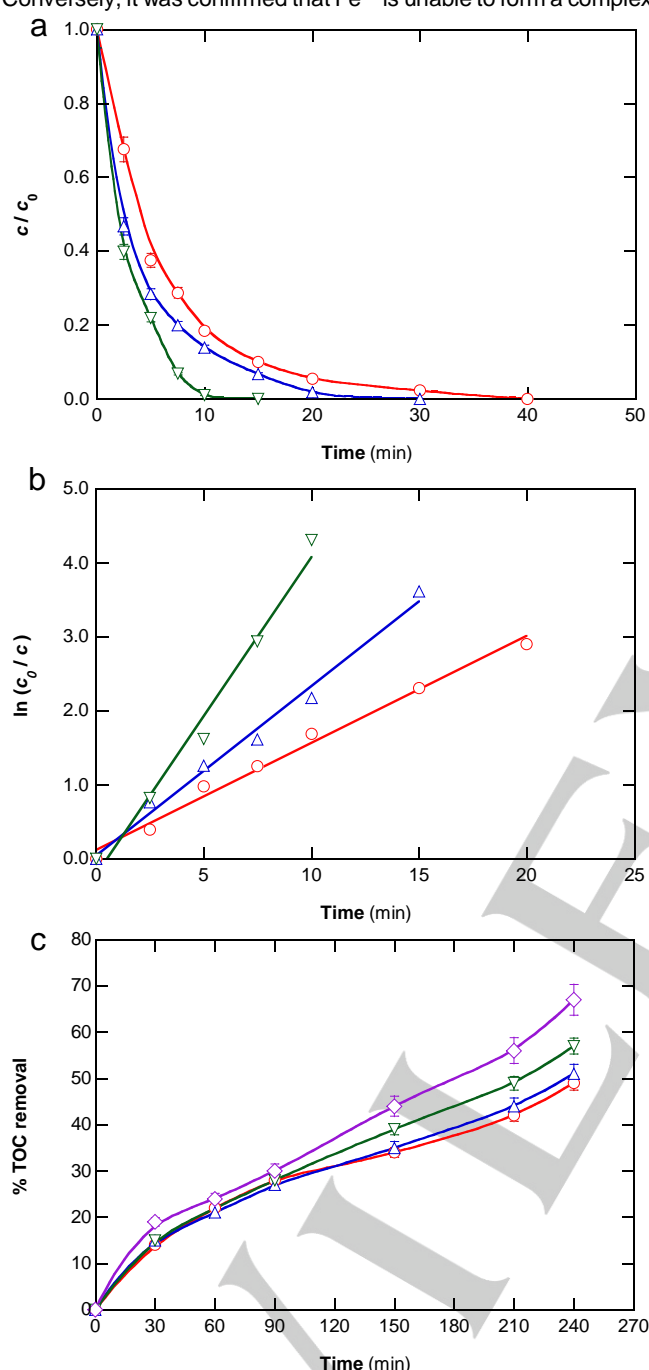


**Figure 2.** (a) Decay of 4-AA concentration with electrolysis time for the treatment of 100 mL of a 50 mg L<sup>-1</sup> 4-AA solution with 0.050 M Na<sub>2</sub>SO<sub>4</sub> at pH 3.0 and 25 °C using a BDD/air-diffusion cell (3 cm<sup>2</sup> electrode area), at 30 mA cm<sup>-2</sup>. Method: (○) Electrochemical oxidation with electrogenerated H<sub>2</sub>O<sub>2</sub> (EO-H<sub>2</sub>O<sub>2</sub>), (△) electro-Fenton (EF) with 15 mg L<sup>-1</sup> Fe<sup>2+</sup>, and (▽) photoelectro-Fenton (PEF) with 15 mg L<sup>-1</sup> Fe<sup>2+</sup> using a 4-W UVA lamp. (b) Pseudo-first-order kinetic analysis of the above concentration decays. (c) Percentage of TOC removal with electrolysis time for the same trials, along with (◇) PEF with 30 mg L<sup>-1</sup> Fe<sup>2+</sup>.

Based on the above findings, a series of absorbance ( $A$ ) measurements was carried out for solutions containing 0.246 mM 4-AA and  $\text{Fe}^{3+}$  concentration ranging from 48.5  $\mu\text{M}$  to 0.984 mM. The analyses were made at  $\lambda_{\text{max}} = 525$  nm, registering the data 3 min after the preparation of the mixtures, that is, when the maximum absorbance values were obtained. Figure 1b evidences the existence of two consecutive linear profiles when  $A_{525}$  is plotted against the  $[\text{Fe}^{3+}]/[4\text{-AA}]$  molar ratio. The  $A$  value rose rapidly upon  $[\text{Fe}^{3+}]/[4\text{-AA}]$  increase up to ca. 2, due to the gradually greater chelation of the metal ions with the drug. At  $[\text{Fe}^{3+}]/[4\text{-AA}]$  values greater than 2, the increase of  $A$  became much slower because almost all drug molecules formed a complex with iron ions. This means that the stoichiometry of the Fe(III)-4-AA complex was 1:2. The complexation constant ( $K$ ) was then determined from the following equation:<sup>[45]</sup>

$$\frac{A_0}{A-A_0} = \frac{\varepsilon_0}{\varepsilon - \varepsilon_0} + \frac{\varepsilon_0}{\varepsilon - \varepsilon_0} \frac{1}{K [\text{Fe}^{3+}]} \quad (6)$$

where  $A_0$  and  $A$  denote the absorbance in the absence and presence of Fe(III), respectively, and  $\varepsilon_0$  and  $\varepsilon$  are the molar absorption coefficients of the corresponding solutions. From the good linear correlation between  $A_0/(A - A_0)$  and  $1/[\text{Fe}^{3+}]$  depicted in Figure 1c ( $R^2 = 0.993$ ) taking all the data shown in Figure 1b,  $K = 6.2 \times 10^6 \text{ M}^{-1}$  was determined, a value very close to  $7.1 \times 10^6 \text{ M}^{-1}$  found in earlier work by potentiometric titration.<sup>[44]</sup>

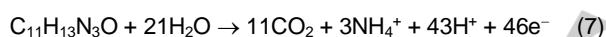
## 2.2 Comparative treatment of 4-AA solutions by EAOPs

To clarify whether PEF with a BDD anode is the most powerful EAOP for 4-AA removal, a comparative study with 50 mg L<sup>-1</sup> drug solutions in the presence of 0.050 M Na<sub>2</sub>SO<sub>4</sub> at pH 3.0 (optimal for Fenton's reaction (2)) was performed by EO-H<sub>2</sub>O<sub>2</sub>, EF, and PEF, with only 15 mg L<sup>-1</sup> Fe<sup>2+</sup> as catalyst for both Fenton-based methods, at a current density of 30 mA cm<sup>-2</sup>. A fast 4-AA removal by all these processes can be observed in Figure 2a, disappearing after 40, 30, and 15 min of EO-H<sub>2</sub>O<sub>2</sub>, EF, and PEF, respectively. The drug decay by EO-H<sub>2</sub>O<sub>2</sub> is due to the attack of BDD(\*OH) formed from reaction (3). The additional \*OH generation from Fenton's reaction (2) explains the quicker 4-AA drop in EF, probably with a small contribution from the destruction of the unstable complex formed between Fe(III), produced from the above reaction, and 4-AA. The much larger enhancement of drug decay in PEF can then be mainly ascribed to other two concomitant factors: (i) the larger production of \*OH, as a result of photolytic reaction (4), and (ii) the direct photolysis of the Fe(III)-4-AA complex. The analysis of these concentration abatements obeyed a pseudo-first-order reaction kinetics, as shown in Figure 2b. From these plots, an increasing apparent rate constant ( $k_1$ ) of 0.145 min<sup>-1</sup> ( $R^2 = 0.989$ ) for EO-H<sub>2</sub>O<sub>2</sub>, 0.229 min<sup>-1</sup> ( $R^2 = 0.988$ ) for EF, and 0.429 min<sup>-1</sup> ( $R^2 = 0.983$ ) for PEF, was obtained. This

behavior is indicative of a steady drug removal in each treatment, suggesting a constant BDD(\*OH) and/or \*OH production, at least during the first stage.

Figure 2c depicts a slight gradual enhancement of TOC removal with time for the above series of experiments, attaining 49%, 51%, and 57% after 240 min of EO-H<sub>2</sub>O<sub>2</sub>, EF, and PEF, respectively. These results confirm again the superiority of PEF over the other EAOPs. Nevertheless, its performance depends on the ability of \*OH production. This can be deduced from the higher TOC abatement, up to 67%, achieved when a greater Fe<sup>2+</sup> content of 30 mg L<sup>-1</sup> was initially employed to treat the 50 mg L<sup>-1</sup> drug solution (Figure 2c). This resulted from the acceleration of Fenton's reaction (2), yielding greater amounts of \*OH as well as of Fe<sup>3+</sup> at a given time that increased the quantity of photoactive products and caused a quicker photolysis. The optimization of the PEF process is then crucial to reach the highest efficiency.

The mineralization of the 50 mg L<sup>-1</sup> 4-AA solution is expected to transform its N atoms mainly into nitrogenated ions.<sup>[19,21]</sup> The analysis of the final solution with 30 mg L<sup>-1</sup> Fe<sup>2+</sup> after 410 min of PEF, where 97% TOC was abated, revealed the release of 0.78 mM NH<sub>4</sub><sup>+</sup> ion (82.5% of initial N) and 0.24 mM NO<sub>3</sub><sup>-</sup> ion (7.3% of initial N). From these data, the overall mineralization reaction for the drug, considering NH<sub>4</sub><sup>+</sup> as the pre-eminent nitrogenated ion, can be written as follows with an *n*-value of 46:



This allowed the estimation of the percentage of mineralization current efficiency (MCE) for each assay from equation (8).<sup>[19]</sup>

$$MCE (\%) = \frac{n F V_s \Delta TOC}{4.32 \times 10^7 m I t} 100 \quad (8)$$

where *F* is the Faraday constant, *V<sub>s</sub>* is the solution volume (in L), ΔTOC is the change of TOC (in mg L<sup>-1</sup>), 4.32 × 10<sup>7</sup> is a conversion factor (3600 s h<sup>-1</sup> × 12,000 mg C mol<sup>-1</sup>), *m* = 11 is the number of carbon atoms of 4-AA, *I* is the current (in A), and *t* is the electrolysis time (in h).

## 2.3 Optimization of the PEF process by response surface methodology

### 2.3.1 Central composite desing (CCD) model

The influence of the main independent variables on several characteristic parameters of the PEF treatment of 4-AA in 0.050 M Na<sub>2</sub>SO<sub>4</sub> solutions at pH 3.0 was assessed with a CCD model based on response surface methodology. The four selected independent variables were: current density (*X*<sub>1</sub>), initial Fe<sup>2+</sup> concentration (*X*<sub>2</sub>), initial 4-AA concentration (*X*<sub>3</sub>), and electrolysis

**Table 1.** Levels of the 2<sup>4</sup> central composite design (CCD) for the PEF treatment of 4-AA.

Variable	Level				
	-2	-1	0	+1	+2
Current density (mA cm <sup>-2</sup> ), <i>X</i> <sub>1</sub>	10.0	32.5	55.0	77.5	100.0
[Fe <sup>2+</sup> ] (mg L <sup>-1</sup> ), <i>X</i> <sub>2</sub>	2.0	17.25	32.5	47.75	63.0
[4-AA] (mg L <sup>-1</sup> ), <i>X</i> <sub>3</sub>	25.0	62.5	100.0	137.5	175.0
Time (min): % 4-AA degradation, <i>X</i> <sub>4</sub>	1	3	5	7	9
Time (min): % 4-AA mineralization and % MCE, <i>X</i> <sub>4</sub>	10	50	90	130	170

time (*X*<sub>4</sub>). A 2<sup>4</sup> factorial design was then followed, with a total of 27 trials involving 16 cube points, 8 axial points, and a triplicate at the center point, and the experimental matrix was generated with the Statistica 10 software (StatSoft, Tulsa, USA). Table 1 collects the experimental levels and ranges chosen for the four independent variables to evaluate the performance from the percentages of 4-AA degradation, 4-AA mineralization, and MCE. Based on Figure 2, short times were selected for the former percentage, being much longer for the two latter ones. Table 2 summarizes the observed results for the twenty-seven selected assays, whose experimental parameters are listed in Table S1.

From the response surface methodology, the following second-order polynomial equation was deduced to describe the interaction between independent and dependent variables:<sup>[14,47]</sup>

$$Y = \beta_0 + \sum_{i=1}^k \beta_i X_i + \sum_{1 \leq i \leq j}^k \beta_{ij} X_i X_j + \sum_{i=1}^k \beta_{ii} X_i^2 \quad (9)$$

where *k* represents the number of variables, *Y* denotes the dependent variable (percentage of 4-AA degradation, 4-AA mineralization, or MCE), and β<sub>0</sub>, β<sub>*i*</sub>, β<sub>*ij*</sub>, and β<sub>*ii*</sub> denote the regression coefficients for the linear and quadratic effects related to the linear *X<sub>i</sub>*, quadratic *X<sub>i</sub><sup>2</sup>*, and *X<sub>i</sub>X<sub>j</sub>* interaction terms.

Table 2 also collects the predicted responses generated from equation (9) for the arithmetic averages of the three dependent variables with ±95% confidence limits. Figures S1a, S1c, and S1e depict the excellent linear predicted-observed values plots obtained for the percentages of 4-AA degradation, 4-AA mineralization, and MCE, respectively. These linear relationships present good *R*<sup>2</sup>-values between 0.963 and 0.975, as well as adjusted correlation coefficients (*R*<sup>2</sup><sub>adj</sub>) between 0.919 and 0.945. The model was then validated from the good accordance between the predicted and observed values.<sup>[14,47]</sup> Moreover, Figures S1b, S1d, and S1f evidence that the corresponding expected normal value vary linearly with the residuals, i.e., the difference between the predicted and observed values. This informs about the sturdiness of the three mathematic models, following a normal distribution and allowing describing appropriately the responses.<sup>[47-49]</sup>

## ARTICLE

**Table 2.** Observed and predicted values of the percentage of degradation, mineralization, and mineralization current efficiency, obtained for the PEF treatment of 4-AA using different combinations of the 2<sup>4</sup> CCD. The experimental parameter for each level in each trial is given in Table S1.

Trial	% 4-AA degradation		% 4-AA mineralization		% MCE	
	Obs.	Pred.	Obs.	Pred.	Obs.	Pred.
1	31	27	11	10	4.5	5.0
2	64	61	24	24	2.4	2.8
3	14	12	4.0	5.0	4.7	6.3
4	56	52	15	13	2.2	3.2
5	45	44	14	15	5.8	7.5
6	78	75	32	35	4.9	2.7
7	18	15	12	10	12	11
8	55	52	25	24	9.8	9.0
9	47	44	11	13	2.4	3.8
10	70	67	30	31	2.4	2.5
11	27	23	15	11	5.8	4.7
12	57	52	24	23	3.7	2.6
13	79	76	19	20	3.8	2.8
14	99	95	45	44	3.2	2.1
15	43	40	16	17	6.3	6.4
16	70	67	35	35	5.4	4.8
17	18	23	11	11	12	10
18	46	54	26	26	2.9	5.7
19	18	27	16	17	3.0	4.4
20	52	57	35	34	6.0	1.9
21	85	91	28	25	1.8	1.9
22	40	47	9.0	12	3.8	5.4
23	17	22	2.0	3.0	9.1	7.1
24	75	82	35	35	3.2	6.4
25	48	47	20	20	4.1	6.3
26	48	47	18	20	4.1	6.3
27	46	47	21	20	4.5	6.3

## 2.3.2 4-AA degradation percentage

The Pareto chart of Figure 3a obtained for the percentage of 4-AA degradation highlights the statistical significance ( $p > 0.05$ ) of

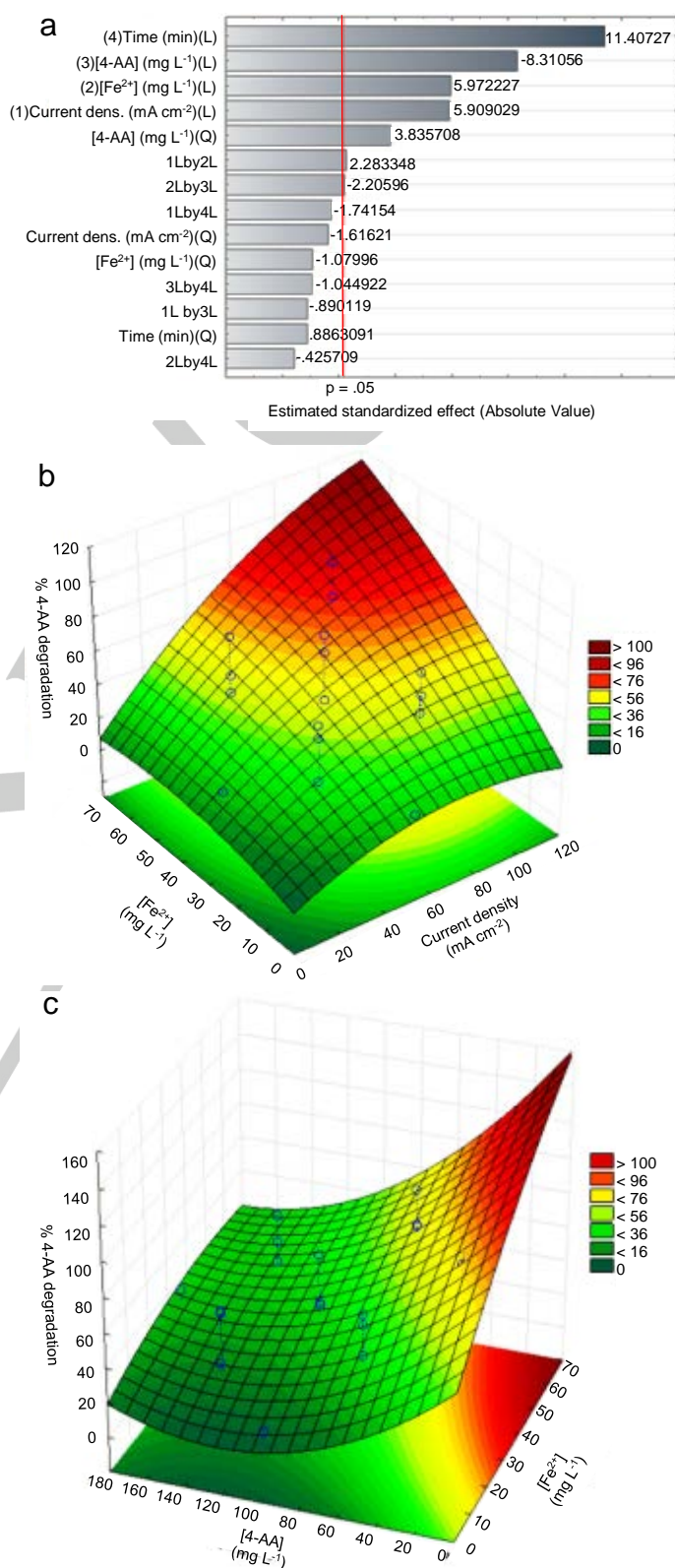


**Figure 3.** (a) Pareto chart for the percentage of 4-AA degradation. Response surface plots for such percentage vs.: (b) current density and Fe<sup>2+</sup> content at 62.5 mg L<sup>-1</sup> drug, and (c) Fe<sup>2+</sup> and 4-AA concentration at current density of 77.5 mA cm<sup>-2</sup>, after 3 min of PEF treatment.

the four linear independent parameters, the squared initial drug concentration, and the interactions of initial  $\text{Fe}^{2+}$  content with current density (1Lby2L) and initial 4-AA concentration (2Lby3L). The following empirical equation was derived from the model, only considering the terms that are statistically significant:

$$Y_{\% \text{degr}} = 47.3 + 15.6X_1 + 15.7X_2 - 21.9X_3 + 10.7X_3^2 + 30X_4 + 7.4X_1X_2 - 7X_2X_3 \quad (10)$$

where  $Y_{\% \text{degr}}$  represents the response of the percentage of 4-AA degradation, whereas  $X_1$ ,  $X_2$ ,  $X_3$ , and  $X_4$  denote the linear variables current density, initial  $\text{Fe}^{2+}$  concentration, initial 4-AA content, and time, respectively.

It is important to pay attention to the signs of the regression coefficients, since a positive value is indicative of an improvement of the response with increasing the dependent variable, whereas the opposite trend occurs for a negative coefficient. For the interacted variables, positive coefficients reveal a synergistic effect, whereas negative ones reveal an antagonistic influence between them.<sup>[50,51]</sup> According to equation (10), these criteria evidence an increase in the percentage of drug degradation with increasing current density, initial  $\text{Fe}^{2+}$  concentration, and time. This agrees with the concomitant production of greater quantities of  $\text{BDD}(\cdot\text{OH})$  from reaction (3) at high current, as well as of  $\cdot\text{OH}$  by accelerating reaction (1), leading to higher amounts of  $\text{H}_2\text{O}_2$  that enhance Fenton's reaction (2).<sup>[19,21]</sup> The quicker  $\text{Fe}^{3+}$  reduction to  $\text{Fe}^{2+}$  at the cathode also favors the latter reaction.<sup>[20]</sup> Independently, Fenton's reaction (2) can be upgraded when greater  $\text{Fe}^{2+}$  amounts are added to the medium, with faster production of  $[\text{Fe}(\text{OH})]^{2+}$  that can photogenerate more  $\cdot\text{OH}$  from reaction (4).<sup>[19,23]</sup> The progressive degradation of drug molecules explains the positive effect of time since longer time allows their gradual oxidation. Conversely, the highly negative coefficient related to 4-AA concentration accounted for a more rapid abatement of smaller amounts of drug, since the same content of oxidizing agents are expected to be formed under analogous conditions, thus limiting the molecule destruction.<sup>[21,23]</sup> However, a positive coefficient was determined for the squared 4-AA concentration, in agreement with a rotatability model.<sup>[52,53]</sup>

A synergistic effect can be observed in equation (10) for the interaction between current density and initial  $\text{Fe}^{2+}$  concentration, with positive coefficient. This important feature can be easily deduced from Table 2 for 62.5 mg  $\text{L}^{-1}$  drug electrolysis at 3 min, attaining 31% degradation at 32.5 mA  $\text{cm}^{-2}$  with 17.25 mg  $\text{L}^{-1}$   $\text{Fe}^{2+}$ , which grew to 79% by increasing both variables to 77.5 mA  $\text{cm}^{-2}$  and 47.75 mg  $\text{L}^{-1}$   $\text{Fe}^{2+}$ . The negative coefficient of the relationship of initial  $\text{Fe}^{2+}$  and 4-AA contents informs about their antagonistic effect, causing a loss of percentage degradation when both parameters grew simultaneously. For example, after 3 min at 77.5 mA  $\text{cm}^{-2}$ , the 4-AA removal reached 47% at 17.25 mg  $\text{L}^{-1}$   $\text{Fe}^{2+}$  and 62.5 mg  $\text{L}^{-1}$  drug, dropping to 43% when the variables increased to 47.75 mg  $\text{L}^{-1}$   $\text{Fe}^{2+}$  and 137.5 mg  $\text{L}^{-1}$  drug. Figures 3b and c show the response surfaces generated for both pairs of independent

variables at 3 min of treatment. For 62.5 mg  $\text{L}^{-1}$  4-AA, Figure 3b depicts a small drug removal operating either at the lowest current density of 10.0 mA  $\text{cm}^{-2}$  or the smallest  $\text{Fe}^{2+}$  concentration of 17.25 mg  $\text{L}^{-1}$ , with a drastic enhancement upon increase of both variables as a result of the gradual acceleration of oxidants production, as stated above. A high degradation of 79% was already attained at 77.5 mA  $\text{cm}^{-2}$  and 47.75 mg  $\text{L}^{-1}$   $\text{Fe}^{2+}$ . Considering the latter current density, the opposite influence of  $\text{Fe}^{2+}$  and 4-AA contents on degradation percentage can be seen in Figure 3c, since it was upgraded with raising the former variable but decreased with increasing the latter one. For example, at the highest drug concentration of 137.5 mg  $\text{L}^{-1}$ , 27% degradation was achieved using 17.25 mg  $\text{L}^{-1}$   $\text{Fe}^{2+}$ , increasing to 43% at higher 47.75 mg  $\text{L}^{-1}$   $\text{Fe}^{2+}$ . In contrast, a much greater degradation of 79% was reached at a lower drug content of 62.5 mg  $\text{L}^{-1}$  using the latter  $\text{Fe}^{2+}$  value. A look to Tables 2 and S1 confirms that the best degradation conditions were attained at 77.5 mA  $\text{cm}^{-2}$ , 47.75 mg  $\text{L}^{-1}$   $\text{Fe}^{2+}$ , and 62.5 mg  $\text{L}^{-1}$  4-AA, with 99% drug removal in 7 min.

### 2.3.3 4-AA mineralization percentage

When the percentage of 4-AA mineralization ( $Y_{\% \text{miner}}$ ) in the PEF treatment was considered, the four linear variables, the squared initial  $\text{Fe}^{2+}$  concentration, and the interactions between time and initial  $\text{Fe}^{2+}$  (2Lby4L) or initial 4-AA (3Lby4L) contents presented a p-value > 0.05, then resulting statistically significant, as can be seen in the corresponding Pareto chart of Figure 4a. The generated empirical model for  $Y_{\% \text{miner}}$  expressed as a function of the different  $X_i$  terms above defined, only considering the terms that are statistically significant, can be expressed as follows:

$$Y_{\% \text{miner}} = 19.7 + 7.3X_1 + 8.5X_2 + 3.1X_2^2 - 6.5X_3 + 16.17X_4 + 3X_2X_4 - 3X_3X_4 \quad (11)$$

According to this equation, increasing current density, the initial  $\text{Fe}^{2+}$  concentration and its square, as well as time improved the mineralization of the drug solutions, as revealed by the positive coefficients. This is the same behavior described above for the percentage of degradation and it is related to the gradually greater production of  $\text{BDD}(\cdot\text{OH})$  and  $\cdot\text{OH}$  from reactions (1)-(4) as the values of these variables were increased. Furthermore, the quicker generation of photoactive products accelerated their photodecomposition under UVA illumination, upgrading the mineralization process. The positive coefficient of the quadratic  $\text{Fe}^{2+}$  concentration agrees again with the prediction of a rotatability model. Longer time was also beneficial. However,  $\text{Fe}^{2+}$  reached a maximum concentration, since its excess causes its destruction with  $\cdot\text{OH}$  to form  $\text{Fe}^{3+}$  and  $\text{OH}^-$ .<sup>[19-23]</sup> The opposite trend occurred for 4-AA concentration, with a negative coefficient in equation (11), in agreement with the limited formation of oxidizing species under given conditions.

Equation (11) shows a synergistic effect of the initial  $\text{Fe}^{2+}$  content and time, presupposing greater mineralization with the rise of both

variables. For example, using  $77.5 \text{ mA cm}^{-2}$  and  $62.5 \text{ mg L}^{-1}$  drug, 30% mineralization was attained after 130 min of electrolysis with  $17.24 \text{ mg L}^{-1} \text{ Fe}^{2+}$ , which increased to 45% at the same time with  $47.75 \text{ mg L}^{-1} \text{ Fe}^{2+}$  (Table 2). On the other hand, the initial 4-AA concentration vs. time relationship presented an antagonistic effect with negative coefficient. The effects of the above synergistic and antagonistic interactions on the mineralization percentage can be visualized in the corresponding response surfaces presented in Figures 4b and c. The best experimental conditions were:  $77.5 \text{ mA cm}^{-2}$ ,  $47.75 \text{ mg L}^{-1} \text{ Fe}^{2+}$ , and  $62.5 \text{ mg L}^{-1}$  4-AA, which yielded up to 96% mineralization by extending the electrolysis to 410 min. This demonstrates the high oxidation ability of PEF to destroy all the oxidation products of the drug due to the combined action of  $\text{BDD}(\cdot\text{OH})$ ,  $\cdot\text{OH}$ , and UVA light.

### 2.3.4 Percentage of mineralization current efficiency

Regarding the percentage of MCE ( $Y_{\%MCE}$ ), the Pareto chart of Figure 5a evidences that the four variables, the quadratic current density, and the relationship between current density and initial  $\text{Fe}^{2+}$  concentration (1LbyL2) show statistical significance ( $p > 0.05$ ). The following equation represents the effect of the variables  $X_i$  above defined on  $Y_{\%MCE}$ , only considering the terms that are statistically significant:

$$Y_{\%MCE} = 4.28 - 2.67X_1 + 1.58X_1^2 + 2.34X_2 + 2X_3 - 1.89X_4 - 1.74X_1X_2 \quad (12)$$

The negative coefficients of current density and time indicate that they are inversely proportional to the percentage of MCE, causing a decrease of this parameter when those variables increased. This tendency is in contrast to that of the quadratic current density, as well as initial  $\text{Fe}^{2+}$  and drug concentrations, with positive coefficients. This can be related to the enhancement of the parasitic reactions involving  $\text{BDD}(\cdot\text{OH})$  and  $\cdot\text{OH}$ , with loss of MCE in the former case, whereas in the second one, the deceleration of such reactions allows the greater production of oxidizing species that upgrade the destruction of organic pollutants.<sup>[19,21,23]</sup> Some examples from the data listed in Tables 2 and S1 can justify the trends given by equation (12). At  $32.5 \text{ mA cm}^{-2}$ , 5.0% MCE was obtained at 50 min for the treatment of  $62.5 \text{ mg L}^{-1}$  with  $17.25 \text{ mg L}^{-1} \text{ Fe}^{2+}$ . When the current density grew to  $77.5 \text{ mA cm}^{-2}$ , the MCE value decreased to 3.8%, which decayed to 2.5% at a longer time of 130 min. Conversely, the MCE increased to 11% operating with  $47.75 \text{ mg L}^{-1} \text{ Fe}^{2+}$ , and to 6.3% at  $137.5 \text{ mg L}^{-1}$  4-AA, always maintaining the values of the other variables.

An antagonistic relationship between current density and initial  $\text{Fe}^{2+}$  concentration is also shown in equation (12). This can be observed in the response surface of the percentage of MCE with both variables, as presented in Fig. 5b, where its value increased with decreasing current density and raising  $\text{Fe}^{2+}$  content. For the best degradation and mineralization conditions ( $77.5 \text{ mA cm}^{-2}$ ,  $47.75 \text{ mg L}^{-1} \text{ Fe}^{2+}$ , and  $62.5 \text{ mg L}^{-1}$  drug), discrete observed and

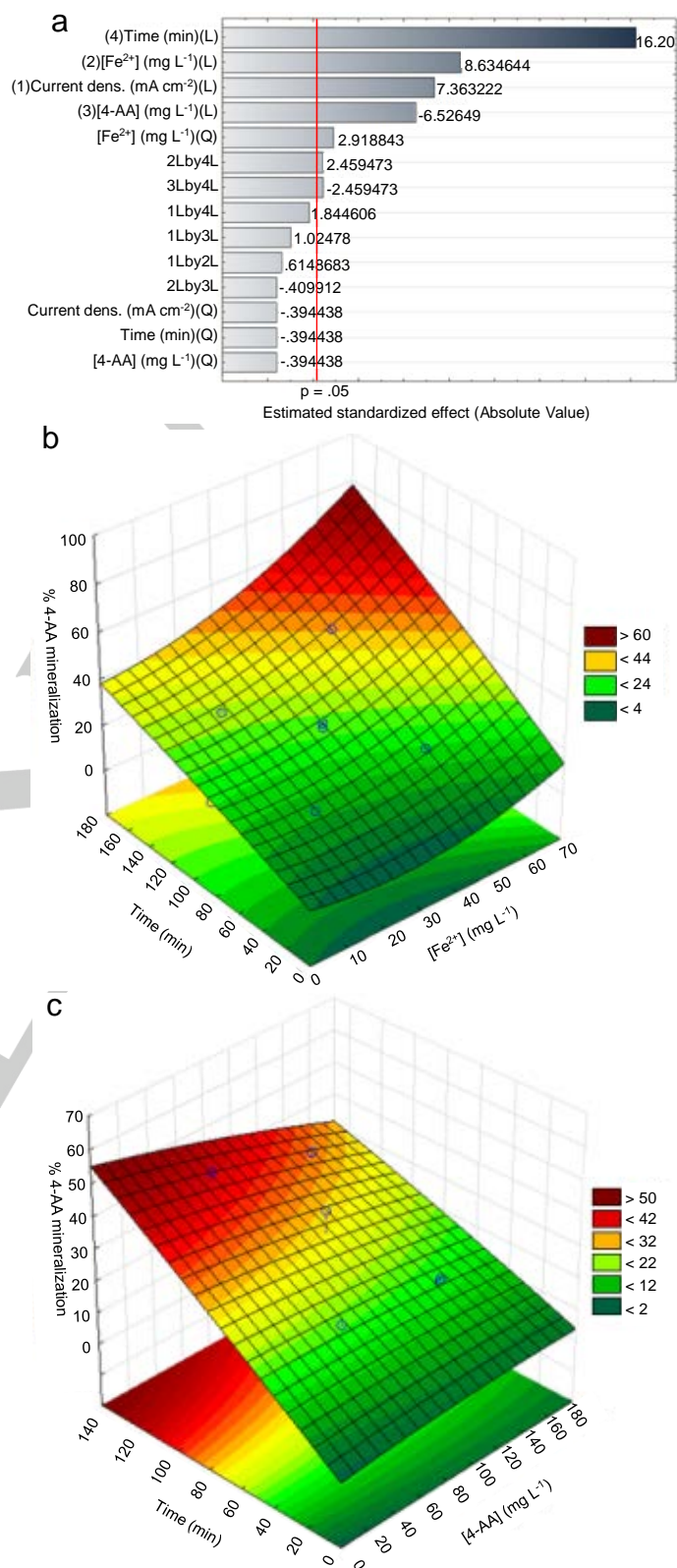


**Figure 4.** (a) Pareto chart for the percentage of 4-AA mineralization. Response surface plot for this percentage vs.: (b)  $\text{Fe}^{2+}$  content and time at  $62.5 \text{ mg L}^{-1}$  drug, and (c) 4-AA concentration and time at  $47.75 \text{ mg L}^{-1} \text{ Fe}^{2+}$ , upon PEF treatment at current density of  $77.5 \text{ mA cm}^{-2}$ .

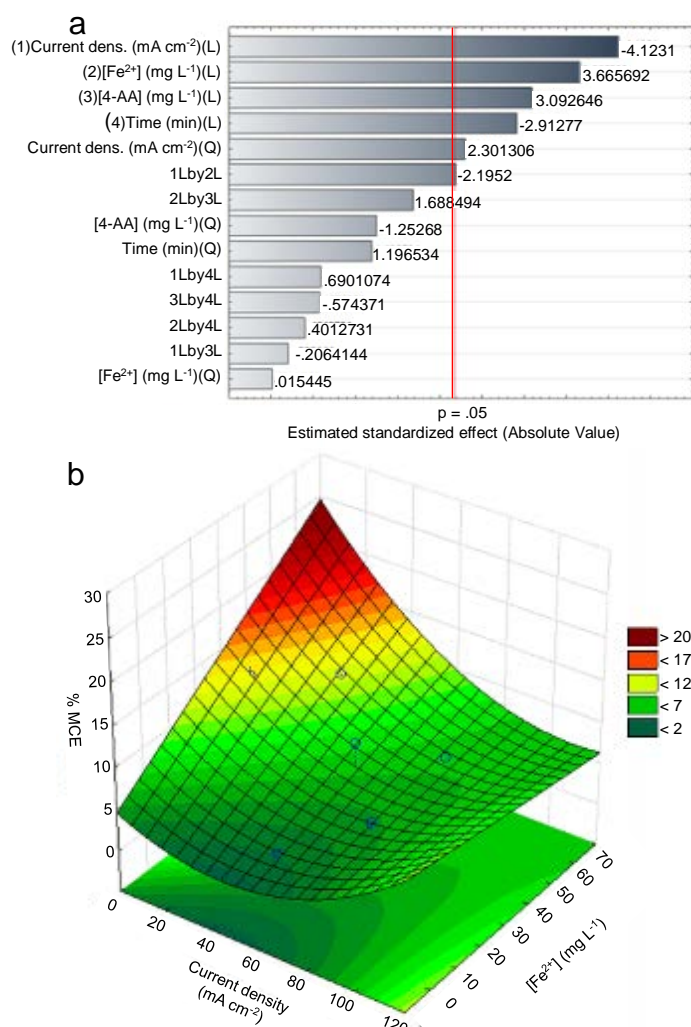


**Figure 5.** (a) Pareto chart for the percentage of mineralization current efficiency. (b) Response surface plot for such percentage vs.  $\text{Fe}^{2+}$  concentration and current density, upon PEF treatment of solutions with  $137.5 \text{ mg L}^{-1}$  drug for 50 min.

predicted MCE values of 3.2% and 2.1%, respectively, were determined at 130 min (Table 2) because of the relatively high applied current density.

#### 2.4 PEF treatment of 4-AA in a municipal secondary effluent

Once established the best operational variables ( $62.5 \text{ mg L}^{-1}$  4-AA, current density of  $77.5 \text{ mA cm}^{-2}$  and  $47.75 \text{ mg L}^{-1}$   $\text{Fe}^{2+}$ ) for the PEF treatment of 4-AA in pure water with  $0.050 \text{ M Na}_2\text{SO}_4$ , the study was extended under these conditions to a municipal secondary effluent to clarify the effect of its components, natural organic matter (NOM) and inorganic salts, on the process performance. Table S2 collects the physicochemical characteristics of this effluent of pH 7.06, TOC of  $10.5 \text{ mg L}^{-1}$  and  $35.6 \text{ mg L}^{-1}$   $\text{Cl}^-$  as

pre-eminent anion. The presence of  $\text{Cl}^-$  makes the oxidation process more complex because it is oxidized to active chlorine ( $\text{Cl}_2/\text{HClO}$ ) at the BDD surface, which is subsequently transformed into chlorate and perchlorate ions.<sup>[21,23,33]</sup> Competition between active chlorine,  $\text{BDD}(\cdot\text{OH})$  and  $\cdot\text{OH}$  to attack the organic pollutants with generation of chloroderivatives is then expected.

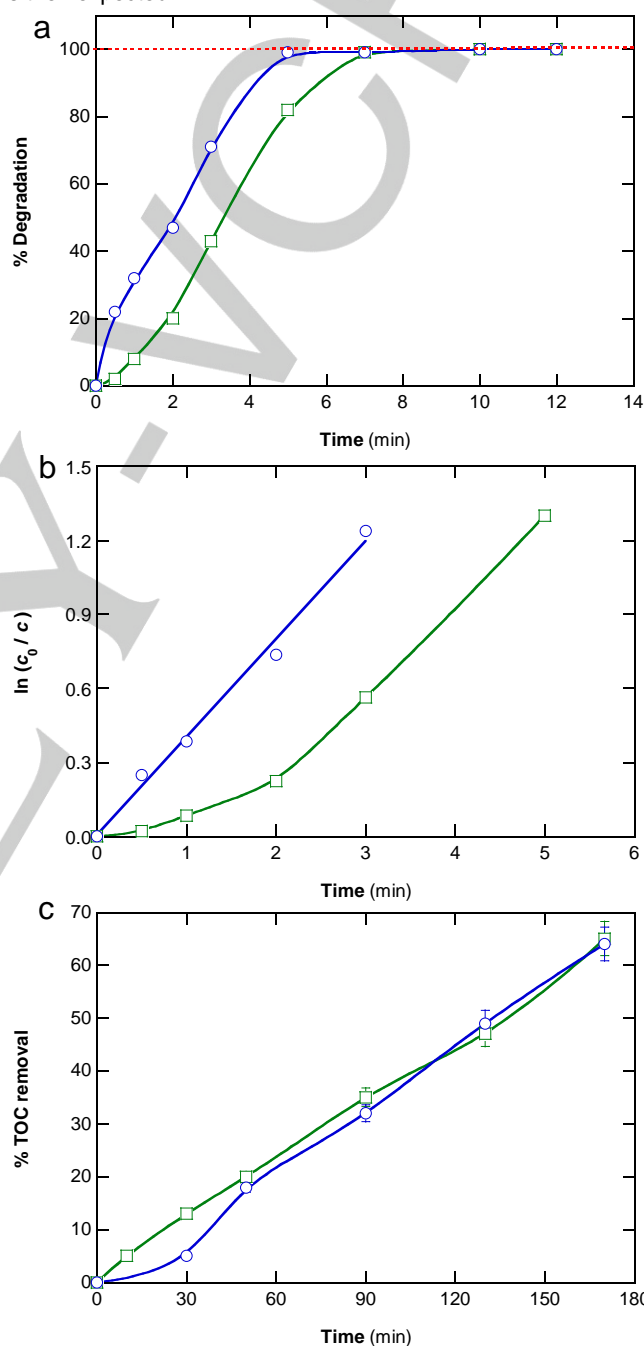


**Figure 6.** (a) Percentage of degradation vs. electrolysis time for the PEF treatment of  $62.5 \text{ mg L}^{-1}$  4-AA in (○) pure water ( $40.6 \text{ mg L}^{-1}$  TOC) and (□) spiked into municipal secondary wastewater ( $51.1 \text{ mg L}^{-1}$  TOC) at pH 3.0,  $25^\circ\text{C}$  and  $77.5 \text{ mA cm}^{-2}$ . In both matrices,  $0.050 \text{ M Na}_2\text{SO}_4$  and  $47.75 \text{ mg L}^{-1}$   $\text{Fe}^{2+}$  were added. (b) Pseudo-first-order kinetic analysis of the above trials. (c) Percentage of TOC removal for the same assays.

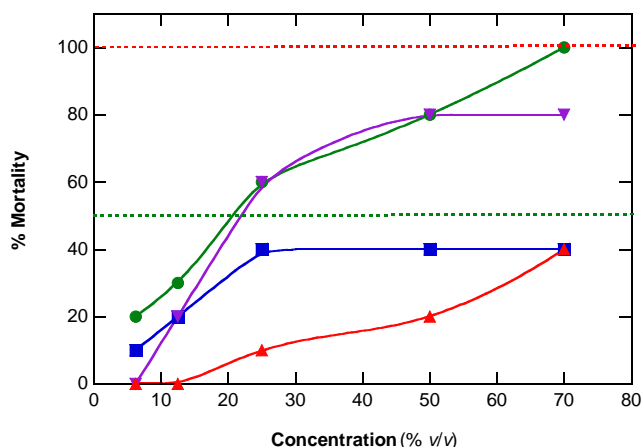


**Figure 7.** (a) Change of *Artemia salina* mortality with the concentration of diluted aliquots of (■) the raw municipal secondary effluent, (●) solutions of 62.5 mg L<sup>-1</sup> of 4-AA spiked into that matrix, and samples withdrawn after (▼) 7 min and (▲) 130 min of PEF treatment of the drug solution in the effluent.

To operate in PEF under the same experimental conditions with both aqueous matrices, 0.050 M Na<sub>2</sub>SO<sub>4</sub> was added to the municipal secondary effluent and its pH was adjusted to 3.0 with H<sub>2</sub>SO<sub>4</sub>. In this way, its conductivity was about 11 mS cm<sup>-1</sup>, very close to that of pure water with 0.050 M Na<sub>2</sub>SO<sub>4</sub>. After spiking the drug and Fe<sup>2+</sup> to reach 62.5 mg L<sup>-1</sup> and 47.75 mg L<sup>-1</sup>, respectively, the PEF treatment of the conditioned municipal secondary effluent at 77.5 mA cm<sup>-2</sup> yielded a similar cell voltage to that of the pure water matrix. Figure 6a shows a slightly slower 4-AA abatement in the former matrix because of the simultaneous oxidation of the drug and NOM with the oxidizing agents, although in both cases > 99% removal was achieved after 7 min. The concentration decay in pure water clearly followed a pseudo-first-order reaction kinetics (Figure 6b), with  $k_1 = 0.393 \text{ min}^{-1}$  ( $R^2 = 0.991$ ), whereas this behavior was not verified using the conditioned municipal secondary effluent due to the consumption of oxidants in NOM degradation. This latter hypothesis was confirmed from the analogous TOC removal percentage obtained using both matrices, as depicted in Fig. 6c. Since 40.6 and 51.1 mg L<sup>-1</sup> TOC were initially contained in pure water and municipal secondary effluent, respectively, one can deduce that after 170 min of electrolysis with 65% TOC reduction, an amount of 26.4 vs. 33.2 mg L<sup>-1</sup> TOC was destroyed during the PEF treatments. The superior quantity of TOC removed in the latter medium corroborated the occurrence of NOM mineralization, which seems to affect rather slightly the drug mineralization. This ensures the good ability of PEF to mineralize 4-AA in municipal secondary effluents.

### 2.5 Acute toxicity assessment

The measurement of the solution toxicity during PEF treatment is essential to limit its duration before a potential combination with a more inexpensive process.<sup>[23]</sup> With this purpose, the larvae of the

microcrustacean *Artemia salina* has been widely used, because it is easy to handle and shows a large acute toxicity to persistent pollutants.<sup>[54,55]</sup> The mortality profile of this organism was then employed to assess the toxicity of: (i) the raw municipal secondary effluent, (ii) a solution of 62.5 mg L<sup>-1</sup> 4-AA prepared with that wastewater, and (iii) the resulting samples after 7 and 130 min of PEF treatment under the best operation conditions. The residual H<sub>2</sub>O<sub>2</sub> in the two latter samples was destroyed by dropwise addition of a solution with 1 g L<sup>-1</sup> catalase.

Figure 7 highlights that the secondary effluent was not acutely toxic, since it did not promote a larval mortality superior to the threshold value of 50%. In contrast, a very high larvae mortality can be observed for the same wastewater contaminated with 4-AA. The median lethal concentration at 50% larvae mortality (LC<sub>50</sub>) can be converted into toxic units (TU) in the 1-10 range from the relationship  $TU = (1/LC_{50}) \times 100$ .<sup>[56]</sup> Thus, a solution with 62.5 mg L<sup>-1</sup> 4-AA spiked into the municipal secondary effluent exhibited an LC<sub>50</sub> = 26.8 mL mL<sup>-1</sup> and TU = 3.8. Similarly, Figure 7 reveals that, after 7 min of PEF, i.e., when the target pollutant was completely removed, the resulting wastewater still presented acute toxicity with LC<sub>50</sub> = 38.6 mL mL<sup>-1</sup> and TU = 2.6. This means that the initially generated oxidation products were still toxic. However, they evolved to much less toxic molecules, as deduced from the fact that, after 130 min of PEF, less than 50% of larvae population was killed (Figure 7). These findings indicate that PEF allows producing non-toxic wastewater upon treatment of water contaminated with 4-AA, at relatively short electrolysis time. Such detoxified wastewater may be further treated by a low cost biological process.

## 3 Conclusions

It has been shown that PEF process with a BDD/air-diffusion cell under irradiation with a 4-W UVA lamp has greater oxidation ability than EF and EO-H<sub>2</sub>O<sub>2</sub> for the removal of 4-AA in 0.050 M Na<sub>2</sub>SO<sub>4</sub> at pH 3.0. This is due to the synergistic oxidative action of UVA photons and generated BDD(\*OH) and \*OH. The formation of an unstable Fe(III)-4-AA complex with 1:2 molar ratio and  $K = 6.2 \times 10^6 \text{ M}^{-1}$  has been evidenced. A 2<sup>4</sup> CCD model, with current density, initial Fe<sup>2+</sup> and drug concentrations, and time as independent variables provided an excellent description of the behavior of the percentages of 4-AA degradation, 4-AA mineralization, and MCE achieved in PEF. The best experimental conditions were: 77.5 mA cm<sup>-2</sup>, 47.75 mg L<sup>-1</sup> Fe<sup>2+</sup>, and 62.75 mg L<sup>-1</sup> 4-AA, giving rise to 99% degradation at 7 min and 45% mineralization at 130 min, along with an MCE of 3.2%. By extending the treatment up to 410 min, the solution attained 96% mineralization. The application of these experimental conditions to the PEF treatment of the drug spiked into a more complex matrix, such as a municipal secondary effluent with 0.050 M Na<sub>2</sub>SO<sub>4</sub> at pH 3.0, revealed a TOC removal of 65% after 240 min, similar to the value obtained in pure water. It has been shown that PEF treatment allows the detoxification of urban wastewater polluted with 4-AA in a short time.

## Experimental Section

Solutions of 4-AA (99% purity, Sigma-Aldrich) in pure water (resistivity > 18.2 MΩ cm, Millipore Milli-Q) were adjusted to pH 3.0 with analytical grade H<sub>2</sub>SO<sub>4</sub> purchased from Vetec Quimica Fina. For the electrolytic assays, analytical grade Na<sub>2</sub>SO<sub>4</sub> and FeSO<sub>4</sub>·7H<sub>2</sub>O purchased from Vetec Quimica Fina were added to the drug solutions as supporting electrolyte and Fenton catalyst, respectively. Prior to acute toxicity analyses, the remaining H<sub>2</sub>O<sub>2</sub> was quenched by adding catalase (10,000-50,000 units per mg of protein, Sigma-Aldrich). All the other reagents used were purchased from Vetec Quimica fina and Sigma-Aldrich, being of HPLC or analytical grade.

Several PEF trials were carried out by spiking 4-AA into a municipal secondary effluent, which was collected from a municipal WWTP located in Campo Grande, the capital of Mato Grosso do Sul state, Brazil. Physicochemical analysis of the above sample, collected in Table S2, was made after filtration with a 10 mm filter. Before use in the electrolytic experiments, the sample was maintained at 4 °C in a refrigerator.

A jacketed, undivided, open, cylindrical glass tank reactor of 150 mL capacity was employed for all the assays. In each experiment, 100 mL of solutions were treated under stirring at 800 rpm, keeping the temperature at 25 °C with thermostated water. The electrolytic trials were performed with a BDD anode and a carbon-PTFE air-diffusion cathode, both of 3 cm<sup>2</sup> geometric area and separated about 1 cm. The BDD anode was a thin film deposited on a single-crystal p-type Si (100) wafer, which was purchased from NeoCoat (La-Chaux-de-Fonds, Switzerland). The air-diffusion cathode was supplied by E-TEK (Somerset, NJ, USA) and was mounted as described elsewhere.<sup>[18]</sup> Compressed air at 1 L min<sup>-1</sup> was directly supplied to it for continuous H<sub>2</sub>O<sub>2</sub> production. The assays were made galvanostatically and the constant current was provided by an Instrutherm Fa-3003 power source. In the PEF experiments, the solutions were illuminated with a Philips TL/4W/08 fluorescent black light blue tube ( $\lambda_{\text{max}}$  = 360 nm) placed 6 cm above their surface. The incident photon intensity of the lamp was of 2.92×10<sup>19</sup> photon s<sup>-1</sup>, as determined by standard potassium ferrioxalate actinometry.<sup>[57]</sup> The surface of both electrodes was previously cleaned and activated upon polarization in 0.050 M Na<sub>2</sub>SO<sub>4</sub> at 300 mA cm<sup>-2</sup> for 180 min.

The solution pH was monitored with a Crison 2000 pH-meter. Once the aliquots were withdrawn from the solutions, they were filtered with Phenomenex 0.45 μm PTFE filters before analysis. Reversed-phase high-performance liquid chromatography (HPLC) was employed to monitor the 4-AA concentration. This analysis was carried out with a Thermo Scientific Finnigan Surveyor system, fitted with an Agilent Technologies Zorbax Eclipse XDB-C-18, 5 μm, 250 mm × 4.6 mm (i.d.) column, and coupled to a photodiode array detector set at  $\lambda = 274$  nm. Filtered samples were diluted (1:1) with acetonitrile (7% NH<sub>3</sub>) to stop the degradation process and further, 25 μL aliquots were injected into the above LC and eluted with a mobile phase composed of a (60:40) methanol/water mixture at 0.5 mL min<sup>-1</sup>. The chromatograms displayed the 4-AA peak at 6.5 min (LOD = 0.025 mg L<sup>-1</sup>). The analysis of dissolved TOC was employed to monitor the drug mineralization. It was measured on a Shimadzu TOC-V CPN analyzer by injecting 50 μL aliquots after immediate withdrawal of the sample (LOD = 0.053 mg L<sup>-1</sup>). Duplicated assays were made under all degradation and mineralization conditions and the average value is given in each case. The ammonium and nitrate concentrations were obtained from the standard methods SM4500-NH<sub>3</sub> C (titrimetric method) and SM 4500-NO<sub>3</sub><sup>-</sup> E, respectively.<sup>[58]</sup>

The mortality of the larvae of microcrustacean *Artemia salina* was employed to assess the acute toxicity in the raw municipal secondary effluent and the untreated and treated solutions with the pollutant 4-AA.

Tests were performed after hatching of the cystic in aerated synthetic seawater (32 g L<sup>-1</sup>, pH 8–9) for 48 h. They were carried out at 20 °C in duplicate (5 individuals per replicate) using well cell culture plates of 3 mL, with a period involving 8 h dark and 16 h light for 96 h. From counting the dead larvae for five dilutions (70, 50, 25, 12.5 and 6.25 %v/v), LC<sub>50</sub> values within 96 h of exposure were calculated.<sup>[59]</sup> Tests were made after removing the iron of samples at pH 8 upon filtration with 0.45 μm filters.

## Acknowledgements

The authors wish to thank the Brazilian funding agencies: Conselho Nacional de Desenvolvimento Científico e Tecnológico (CNPq), Coordenação de Aperfeiçoamento de Pessoal de Nível Superior (Capes, finance code 001), and Fundação de Apoio ao Desenvolvimento do Ensino, Ciência e Tecnologia do Estado de Mato Grosso do Sul (Fundect). Thanks are extended to the Water and Sewage Utility operating in Campo Grande, Mato Grosso do Sul, for kindly providing the municipal secondary effluent sample. Funding from project CTQ2016-78616-R (AEI/FEDER, EU) is also acknowledged.

**Keywords:** Acute toxicity • 4-Aminoantipyrine • Municipal secondary effluent • Photoelectro-Fenton • Response surface methodology

- [1] M. J. Gómez, C. Sirtori, M., Mezcuca, A. R. Fernández-Alba, A. Agüera, *Water Res.* **2008**, *42*, 2698-2706.
- [2] L. Prieto-Rodríguez, I. Oller, N. Klamerth, A. Agüera, E. M. Rodríguez, S. Malato, *Water Res.* **2013**, *47*, 1521-1528.
- [3] M. C. Campos-Mañas, P. Plaza-Bolaños, J. A. Sánchez-Pérez, S. Malato, A. Agüera, *J. Chromatogr. A* **2017**, *1507*, 84-94.
- [4] E. Brillas, I. Sirés, *TrAC-Trend Anal. Chem.* **2015**, *70*, 112-121.
- [5] A. J. Ebele, M. Abou-Elwafa Abdallah, S. Harrad, *Emerg. Contam.* **2017**, *3*, 1-16.
- [6] X. Hu, J. Yang, C. Yang, J. Zhang, *Chem. Eng. J.* **2010**, *161*, 68-72.
- [7] J. L. Gowda, A. T. Buddanavar, S. T. Nandibewoor, *J. Pharm. Anal.* **2015**, *5*, 231-238.
- [8] P. M. P. Santos, A. M. M. Antunes, J. Noronha, E. Fernandes, A. J. S. C. Vieira, *Eur. J. Med. Chem.* **2010**, *45*, 2258-2264.
- [9] I. Muñoz, A. Rodríguez, R. Rosal, A. R. Fernández-Alba, *Sci. Total Environ.* **2009**, *407*, 1245-1256.
- [10] D. Li, H. -X. Tong, L. Zhang, *Trans. Nonferrous Met. Soc. China* **2013**, *23*, 3306-3311.
- [11] L. M. da Silva, F. Gozzi, I. Sirés, E. Brillas, S. C. De Oliveira, A. Machulek Jr., *Sci. Total Environ.* **2018**, *631-632*, 1079-1088.
- [12] S. Gligorovski, R. Strekowski, S. Barbat, D. Vione, *Chem. Rev.* **2015**, *115*, 13051-13092.
- [13] R. P. Cavalcante, R. F. Dantas, B. Bayarri, O. Gonzalez, J. Giménez, S. Esplugas, A. Machulek Jr., *Appl. Catal. B: Environ.* **2016**, *194*, 111-122.
- [14] L. M. da Silva, R. P. Cavalcante, R. F. Cunha, F. Gozzi, R. F. Dantas, S. C. Oliveira, A. Machulek Jr., *Sci. Total Environ.* **2016**, *573*, 518-531.
- [15] R. Salazar, S. Garcia-Segura, M.S. Ureta-Zañartu, E. Brillas, *Electrochim. Acta* **2011**, *56*, 6371-6379.
- [16] G. Coria, I. Sirés, E. Brillas, J. L. Nava, *Chem. Eng. J.* **2016**, *304*, 817-825.
- [17] N. Flores, P. L. Cabot, F. Centellas, J. A. Garrido, R. M. Rodríguez, E. Brillas, I. Sirés, *J. Hazard. Mater.* **2017**, *321*, 566-575.
- [18] D. R. V. Guelfi, F. Gozzi, I. Sirés, E. Brillas, A. Machulek Jr., S. C. de Oliveira, *Environ. Sci. Pollut. Res.* **2017**, *24*, 6083-6095.
- [19] I. Sirés, E. Brillas, *Environ. Int.* **2012**, *40*, 212-229.

- [20] L. Feng, E. D. Van Hullebusch, M. A. Rodrigo, G. Esposito, M. A. Oturan, *Chem. Eng. J.* **2013**, *228*, 944-964.
- [21] I. Sirés, E. Brillas, M. A. Oturan, M. A. Rodrigo, M. Panizza, *Environ. Sci. Pollut. Res.* **2014**, *21*, 8336-8367.
- [22] M. A. Oturan, J. -J. Aaron, *Crit. Rev. Environ. Sci. Technol.* **2014**, *23*, 2577-2641.
- [23] C. A. Martínez-Huitle, M. A. Rodrigo, I. Sirés, O. Scialdone, *Chem. Rev.* **2015**, *115*, 13362-13407.
- [24] A. Khataee, A. Khataee, M. Fathinia, B. Vahid, S. W. Joo, *J. Ind. Eng. Chem.* **2013**, *19*, 1890-1894.
- [25] A. Khataee, A. Akbarpour, B. Vahid, *J. Taiwan Inst. Chem. Eng.* **2014**, *45*, 930-936.
- [26] N. Daneshvar, S. Aber, V. Vatanpour, M. H. Rasoulifard, *J. Electroanal. Chem.* **2008**, *615*, 165-174.
- [27] M. Panizza, M. A. Oturan, *Electrochim. Acta* **2011**, *56*, 7084-7087.
- [28] M. S. Yahya, N. Oturan, K. El Kacemi, M. El Karbane, C. T. Aravindakumar, M. A. Oturan, *Chemosphere* **2014**, *117*, 447-454.
- [29] F. Sopaj, M. A. Rodrigo, N. Oturan, F. I. Podvorica, J. Pinson, M. A. Oturan, *Chem. Eng. J.* **2015**, *262*, 286-294.
- [30] O. Ganzenko, N. Oturan, I. Sirés, D. Huguenot, E. D. van Hullebusch, G. Esposito, M. A. Oturan, *Environ. Chem. Lett.* **2018**, *16*, 281-286.
- [31] A. Thiam, I. Sirés, E. Brillas, *Water Res.* **2015**, *81*, 178-187.
- [32] A. Thiam, I. Sirés, J. A. Garrido, R. M. Rodríguez, E. Brillas, *Sep. Purif. Technol.* **2015**, *140*, 43-52.
- [33] X. Yu, M. Zhou, G. Ren, L. Ma, *Chem. Eng. J.* **2015**, *263*, 92-100.
- [34] J. R. Steter, E. Brillas, I. Sirés, *Electrochim. Acta* **2016**, *222*, 1464-1474.
- [35] J. R. Steter, E. Brillas, I. Sirés, *Appl. Catal. B: Environ.* **2018**, *224*, 410-418.
- [36] D. R.V. Guelfi, Z. Ye, F. Gozzi, S. C. de Oliveira, A. Machulek Jr., E. Brillas, I. Sirés, *Sep. Purif. Technol.* **2019**, *211*, 637-645.
- [37] A. El-Ghenymy, R. M. Rodríguez, E. Brillas, N. Oturan, M. A. Oturan, *Environ. Sci. Pollut. Res.* **2014**, *21*, 8368-8378.
- [38] A. Galia, S. Lanzalaco, M.A. Sabatino, C. Dispenza, O. Scialdone, I. Sirés, *Electrochim. Commun.* **2016**, *62*, 64-68.
- [39] O. Ganzenko, N. Oturan, D. Huguenot, E. D. van Hullebusch, G. Esposito, M. A. Oturan, *Separ. Purif. Technol.* **2015**, *156*, 987-995.
- [40] A. Thiam, I. Sirés, J. A. Garrido, R. M. Rodríguez, E. Brillas, *J. Hazard Mater.* **2015**, *290*, 34-42.
- [41] F. Sopaj, N. Oturan, J. Pinson, F. Podvorica, M. A. Oturan, *Appl. Catal. B: Environ.* **2016**, *199*, 331-341.
- [42] J. C. Murillo-Sierra, E. Ruiz-Ruiz, L. Hinojosa-Reyes, J. L. Guzmán-Mar, F. Machuca-Martínez, A. Hernández-Ramírez, *Catal. Today* **2018**, *313*, 175-181.
- [43] E. H. Herman, J. Zhang, B. B. Hasinoff, J. R. J. Clark, V. J. Ferrans, *J. Mol. Cell Cardiol.* **1997**, *29*, 2415-2430.
- [44] M. G. A. E. Wahed, M. A. Elmesallamy, H. M. Kater, M. M. E. Gamel, N. A. Khalil, *Arab. J. Chem.* **2011**, *4*, 169-178.
- [45] R. P. Cavalcante, L. R. Sandim, D. Bogo, A. M. J. Barbosa, M. E. Osugi, M. Blanco, S. C. de Oliveira, M. F. C. Matos, A. Machulek Jr., *Environ. Sci. Pollut. Res.* **2013**, *20*, 2352-2361.
- [46] I. P. Pozdnyakov, A. A. Melnikov, R. Šipoš, S. V. Chekalin, J. Šima, *Chem. Phys. Lett.* **2016**, *660*, 209-213.
- [47] M. B. Kasiri, A. R. Khata, *Desalination* **2011**, *270*, 151-159.
- [48] M. A. Bezerra, R. E. Santelli, E. P. Oliveira, L. S. Villar, L. A. Escaleira, *Talanta* **2008**, *76*, 965-977.
- [49] I. M. Savic, M. Savic, M. Iva, S. T. Stojiljkovic, D. G. Gajic, *Energy* **2014**, *77*, 66-72.
- [50] R. F. P. Nogueira, M. C. Oliveira, W. C. Paterlini, *Talanta* **2005**, *66*, 86-91.
- [51] P. Calza, V. A. Sakkas, C. Medana, A. D. Vlachou, F. Dal Bello, T. A. Albanis, *Appl. Catal. B: Environ.* **2013**, *129*, 71-79.
- [52] R. G. Brereton, *Chemometrics. Data Analysis for the Laboratory and Chemical Plant*, Wiley, Chichester, **2003**.
- [53] B. Singh, R. Kumar, N. Ahuja, *Crit. Rev. Ther. Drug Carrier Syst.* **2004**, *22*, 27-105.
- [54] M. Marković, M. Jović, D. Stanković, V. Kovačević, G. Roglič, G. Gojčić-Cvijović, D. Manojlović, *Sci. Total Environ.* **2015**, *505*, 1148-1155.
- [55] D. A. da Silva, R. P. Cavalcante, R. F. Cunha, A. Machulek Jr., S. C. de Oliveira, *Chemosphere* **2018**, *207*, 457-468.
- [56] G. Persoone, B. Marsalek, I. Blinova, A. Torkokne, D. Zarina, L. Manusadzianas, G. Nalecz-Jawecki, L. Tofan, N. Stepanova, L. Tothova, B. Kolar, *Environ. Toxicol.* **2003**, *18*, 395-402.
- [57] A. Machulek Jr., J. E. F. Moraes, C. Vautier-Giongo, C. A. Silverio, L. C. Friedric, C. A. O. Nascimento, *Environ. Sci. Technol.* **2007**, *41*, 8459-8463.
- [58] APHA. *Standard Methods for the Examination of Water and Wastewater*. 22nd ed., American Public Health Association, New York, **2012**.
- [59] L. El Fels, M. Hafidi, Y. Ouhdouch, *Waste Manage.* **2016**, *50*, 194-200.

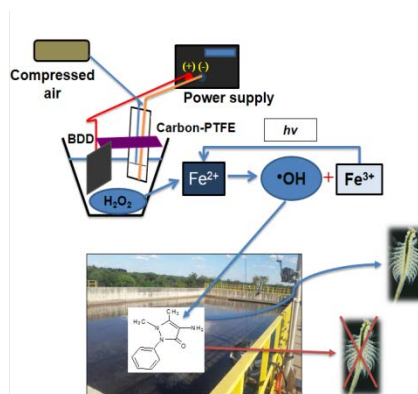
## ARTICLE

## Entry for the Table of Contents (Please choose one layout)

Layout 1:

## ARTICLE

Text for Table of Contents



*L.M da Silva, F. Gozzi, R.P. Cavalcante, S.C. de Oliveira, E. Brillas, I Sirés,\* A. Machulek Jr.\**

**Page No.1 – Page No. 11**

**Treatment of 4-aminoantipyrine by PEF:** The application of PEF process with a BDD anode under UVA illumination is highly efficient for the degradation and mineralization of this pollutant in municipal secondary effluent and provides a decontaminated water without acute toxicity to *Artemia salina*.

Layout 2:

## ARTICLE

((Insert TOC Graphic here))

*Author(s), Corresponding Author(s)\**

**Page No. – Page No.**

**Title**

Text for Table of Contents

---

**SUPPORTING INFORMATION****Assessment of 4-aminoantipyrine degradation and mineralization by photoelectro-Fenton with a BDD anode: Optimization, treatment in municipal secondary effluent, and toxicity**

Lucas de Melo da Silva,<sup>[a]</sup> Fábio Gozzi,<sup>[a]</sup> Rodrigo Pereira Cavalcante,<sup>[a]</sup> Silvio César de Oliveira,<sup>[a]</sup> Enric Brillas,<sup>[b]</sup> Ignasi Sirés,<sup>\*[b]</sup> and Amílcar Machulek Junior<sup>\*[a]</sup>

---

[a] Mr. L.M da Silva, Dr. F. Gozzi, Dr. R.P. Cavalcante, Prof. S.C. de Oliveira, Prof. A. Machulek Jr.  
Institute of Chemistry,  
Federal University of Mato Grosso do Sul  
Av. Senador Filinto Muller, 1555; CP 549; Campo Grande, MS 79074-460, Brazil  
E-mail: machulekjr@gmail.com

[b] Prof. E. Brillas, Prof. I Sirés  
Departament de Química Física  
Facultat de Química, Universitat de Barcelona  
Martí i Franquès 1-11, 08028 Barcelona, Spain  
E-mail: i.sires@ub.edu

---

**Table S1.** Experimental parameters corresponding to the trials given in Table 2.

Trial	Current density (mA cm <sup>-2</sup> )	[Fe <sup>2+</sup> ] (mg L <sup>-1</sup> )	[4-AA] (mg L <sup>-1</sup> )	Time for % 4-AA degradation (min)	Time for % 4-AA mineralization and % MCE (min)
1	32.5	17.25	62.5	3	50
2	32.5	17.25	62.5	7	130
3	32.5	17.25	137.5	3	50
4	32.5	17.25	137.5	7	130
5	32.5	47.75	62.5	3	50
6	32.5	47.75	62.5	7	130
7	32.5	47.75	137.5	3	50
8	32.5	47.75	137.5	7	130
9	77.5	17.25	62.5	3	50
10	77.5	17.25	62.5	7	130
11	77.5	17.25	137.5	3	50
12	77.5	17.25	137.5	7	130
13	77.5	47.75	62.5	3	50
14	77.5	47.75	62.5	7	130
15	77.5	47.75	137.5	3	50
16	77.5	47.75	137.5	7	130
17	10.0	32.5	100.0	5	90
18	100.0	32.5	100.0	5	90
19	55.0	2.0	100.0	5	90
20	55.0	63.0	100.0	5	90
21	55.0	32.5	25.0	5	90
22	55.0	32.5	175.0	5	90
23	55.0	32.5	100.0	1	10
24	55.0	32.5	100.0	9	170
25	55.0	32.5	100.0	5	90
26	55.0	32.5	100.0	5	90
27	55.0	32.5	100.0	5	90

**Table S2.** Physicochemical characteristics of the municipal secondary effluent sample.

Parameter <sup>[a]</sup>	Value
pH	7.06
Conductivity (mS cm <sup>-1</sup> )	2.4
Alkalinity (mg L <sup>-1</sup> )	70
BOD (mg L <sup>-1</sup> )	10.8
COD (mg L <sup>-1</sup> )	40.1
TOC (mg L <sup>-1</sup> )	10.5
Phosphorus (mg L <sup>-1</sup> )	1.72
Ammonia nitrogen (mg L <sup>-1</sup> )	1.4
Kjeldahl nitrogen (mg L <sup>-1</sup> )	4.4
Chloride (mg L <sup>-1</sup> )	35.6
Nitrite (mg L <sup>-1</sup> )	0.7
Nitrate (mg L <sup>-1</sup> )	1.4
Oils and greases (mg L <sup>-1</sup> )	5.8
Suspended Solids (mg L <sup>-1</sup> )	16
Total solids (mg L <sup>-1</sup> )	263
Dissolved Solids (mg L <sup>-1</sup> )	247

[a] Data provided by the Water and Sewage Utility operating in Campo Grande, Mato Grosso do Sul, Brazil.

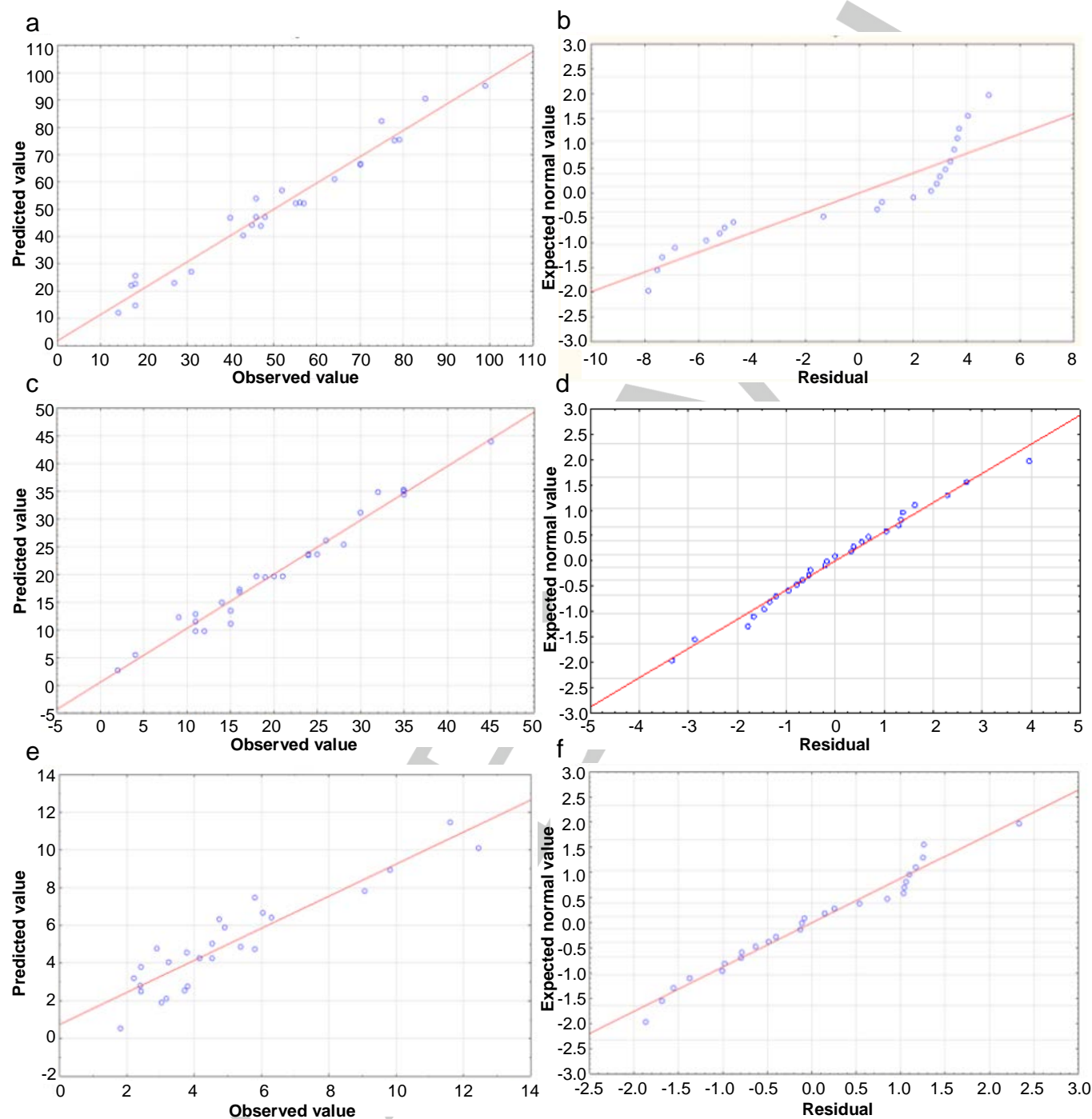


**Figure S1.** Comparison of predicted and observed values for the percentage of: (a) 4-AA degradation, (c) 4-AA mineralization, and (e) mineralization current efficiency. Residual plots for the responses of the percentages of: (b) 4-AA degradation, (d) 4-AA mineralization, and (f) mineralization current efficiency.